Open Ceramics 27 (2026) 101001

Contents lists available at ScienceDirect

Open Ceramics

journal homepage: www.sciencedirect.com/journal/open-ceramics

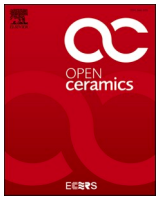

Flash sintering of titanium carbide

Subhadip Bhandari [a,*], Milad Kermani [a], Mattia Biesuz [a], Vincenzo M. Sglavo [a,b]

[a] Department of Industrial Engineering, University of Trento, Via Sommarive 9, Trento, Italy
[b] INSTM, Trento Research Unit, Via G. Giusti 9, Firenze, Italy

ARTICLE INFO

Keywords:
Flash sintering
TiC
TiAl
Liquid-phase sintering

ABSTRACT

In recent years, significant advances have been made in ceramic sintering processes to reduce both the sintering temperature and the time. Notably, flash sintering enables rapid densification within seconds by applying an electric field at significantly lower temperatures than conventional sintering.

In the present work, flash sintering of titanium carbide (TiC) was studied with TiAl as a sintering aid. The results demonstrated that addition of titanium aluminide (TiAl) significantly improves the final density, whereas the application of external pressure during sintering does not have a notable impact on densification. Although the process was carried out in air, the oxidation of TiAl or TiC during sintering was almost negligible, this being correlated with the very limited duration of the process (less than a minute). The present work demonstrates the possibility to produce TiC components very rapidly and without the need of a controlled atmosphere by using the flash sintering technique.

1. Introduction

Over the last two decades, there have been significant developments and advancements in the field of ceramic sintering, with the final goal of decreasing the overall processing time [1,2]. One of the notable advancements was first reported in the form of flash sintering in 2010 by the group of Rishi Raj at the University of Colorado at Boulder (USA) [3]. The study demonstrated that the application of an electric field to 3YSZ samples at 850 °C resulted in a very rapid densification (in less than 5 s). With several well-documented studies, it is possible to conclude that flash occurs at a specific combination of applied electric field and furnace temperature, at which a current begins to flow and triggers a very rapid sintering process due to a thermal runaway phenomenon [4–8]. Flash sintering is typically characterized by three simultaneous events: a non-linear increase in the electrical conductivity of the sample, sudden shrinkage (rapid densification) and bright light emission [9–13].

Most ceramics (ionic conductors, insulators, semiconductors) exhibit a negative temperature coefficient (NTC) for resistivity, which means that the resistance to the flow of current decreases with temperature [9,10]. This reduction in resistivity enables more current to flow through the material, resulting in increased Joule heating. The additional heat further increases the temperature, resulting in an additional decrease in resistivity. In this way, a positive feedback loop is created to activate a thermal runaway process responsible for the very rapid densification of the material [9,10].

Recent studies have demonstrated the possibility of flash sintering in metal-like ceramics that exhibit PTC (positive temperature coefficient for resistivity) behaviour [11–14]. In the green compact, PTC ceramics initially exhibit characteristics of NTC materials due to the limited contact points among the constituting particles, and this is enough to induce the thermal runaway phenomenon [14]. In tungsten carbide green compacts, a reduction in resistivity from 10^{-3} to 10^{-6} Ω m was measured after the application of a limited pressure and the electrical field, and this was sufficient to initiate the thermal runaway and the very rapid heating of the green body [14].

Titanium carbide (TiC) is widely recognized for its exceptionally high melting point, outstanding mechanical properties and moderate thermal conductivity, making it suitable for applications in nuclear power plants, thermal protection systems, cutting and grinding tools, etc. [15,16]. The strong covalent bonding between titanium and carbon leads to a high activation energy for self-diffusion in TiC [17]. As a result, densification of pure titanium carbide requires exceptionally high temperatures of up to around 2300 °C [18]. Some investigations have shown that adding sintering aids such as SiC [17], B_4C [18], Si+ZrC [19], WC [20] etc., can dramatically reduce the sintering temperature.

Most studies have used spark plasma sintering (SPS) or hot pressing (HP) to densify TiC ceramics [17,19–24]. Even in SPS, temperatures

* Corresponding author.
E-mail addresses: subhadip.bhandari@unitn.it, subhadipbhandari@gmail.com (S. Bhandari).

https://doi.org/10.1016/j.oceram.2026.101001
Received 22 April 2026; Received in revised form 8 June 2026; Accepted 8 June 2026
Available online 8 June 2026

over 1800 °C are often required to reach high density [17,21] and the process must be carried out under an inert atmosphere to prevent degradation of the graphite die and, more importantly, the material itself [17,21–24].

Therefore, there is a strong need for alternative processing routes capable of achieving rapid densification and reduced equipment complexity. In this context, flash sintering of titanium carbide remains largely unexplored. With this in mind the goal of the present study was to investigate the feasibility of flash sintering TiC in air at room temperature by using TiAl as a sintering aid because of its chemical compatibility and comparable thermal expansion coefficient [25,26].

2. Materials and methods

2.1. Starting powder

Pure TiC powder as well as TiC powder doped with 10 vol% (denoted as **TiC – 10TiAl**) and 20 vol% (denoted as **TiC – 20TiAl**) of TiAl were synthesized using self-propagating high-temperature synthesis (SHS). This process involves the ignition of powder mixtures (initially with an external source) that undergo an exothermic reaction [27]. Following ignition, the heat generated by the exothermic reaction is continuously transmitted to adjacent reactants, thereby facilitating a self-sustaining combustion wave that propagates across the heterogeneous mixture without external energy input [28,29]. The starting powders were Ti metal > 98 % (William Rowland Ltd. UK), graphite powder 99.6 % (Sofacel, Spain) and Al metal (Alcoa, USA). The characteristics of the powders and details of the synthesis can be found in Ref [22].

The morphology of the starting powders is shown in Fig. 1: regardless of the TiAl content, the powders exhibit an irregular morphology with a particle size of around 2 – 5 μm. The theoretical density of TiC is 4.94 g/cm^3, while the density of the composite powders was calculated using rule of mixtures, and can be approximated as 4.82 g/cm^3 for TiC – 10TiAl, and 4.72 g/cm^3 for TiC – 20TiAl, respectively.

The 10 and 20 vol% TiAl compositions were selected based on previous SPS study [22], which identified TiAl as an effective sintering aid and showed that 20 vol% TiAl yields substantially improved densification compared with lower additions.

2.2. Flash sintering

Flash sintering experiments were carried out on uniaxially pressed cylindrical compacts (~280 MPa) with a nominal diameter of 6 mm and a height of 9.5 mm. The required amount of powder was weighed and homogenized with a drop of deionized water in an agate mortar, which served as a temporary binder after pressing.

Flash sintering experiments were carried out using a custom-made apparatus (Fig. 2) where two copper/molybdenum electrodes were fastened to the load cell and to the actuator connected to the displacement transducer (LVDT) of a universal mechanical testing machine (MTS System, Mod. 810). The green ceramic specimen was placed inside a hexagonal boron nitride (hBN) die and positioned between the upper and lower Mo electrodes. The displacement and the applied force were continuously recorded through the LVDT actuator and the machine load cell. A multichannel data acquisition system (DAQ NI USB-6211) simultaneously acquired voltage and current simultaneously using LabVIEW. The electric power was provided by an AC 50 Hz power supply (TECNA item 3870) connected to the metallic electrodes [30–32]. All flash sintering experiments were carried out in air and the processing conditions (applied voltage, pressure, and duration) are summarized in Table 1. The temperature was measured by pointing a pyrometer (Ultimax infrared thermometer UX −30) through a 4 mm

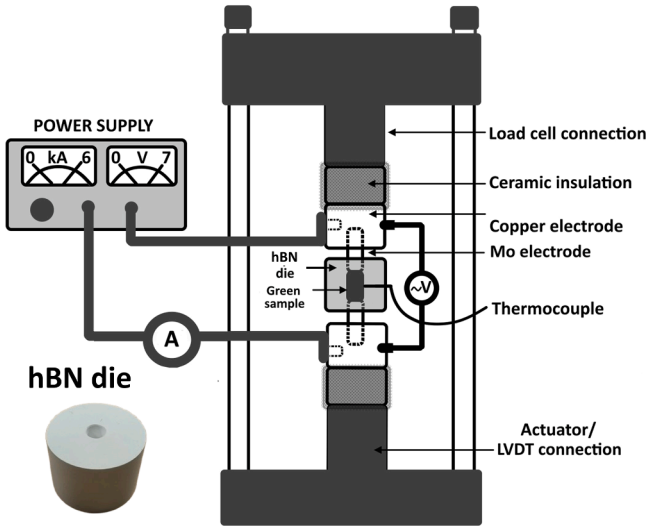

Fig. 2. Experimental setup used to carry out the flash sintering experiments. Reproduced from Ref.: [32], with permission from Elsevier.

Table 1
Flash sintering parameters used for the different compositions.

Experimental parameters	Composition		
	Pure TiC	TiC – 10 TiAl	TiC – 20 TiAl
4.3 V 30 s 40 MPa			✓
4.3 V 60 s 40 MPa			✓
5 V 30 s 10 MPa		✓	✓
5 V 30 s 20 MPa		✓	✓
5 V 30 s 30 MPa		✓	✓
5 V 30 s 40 MPa		✓	✓
5 V 30 s 60 MPa		✓	✓
5 V 60 s 40 MPa	✓	✓	✓

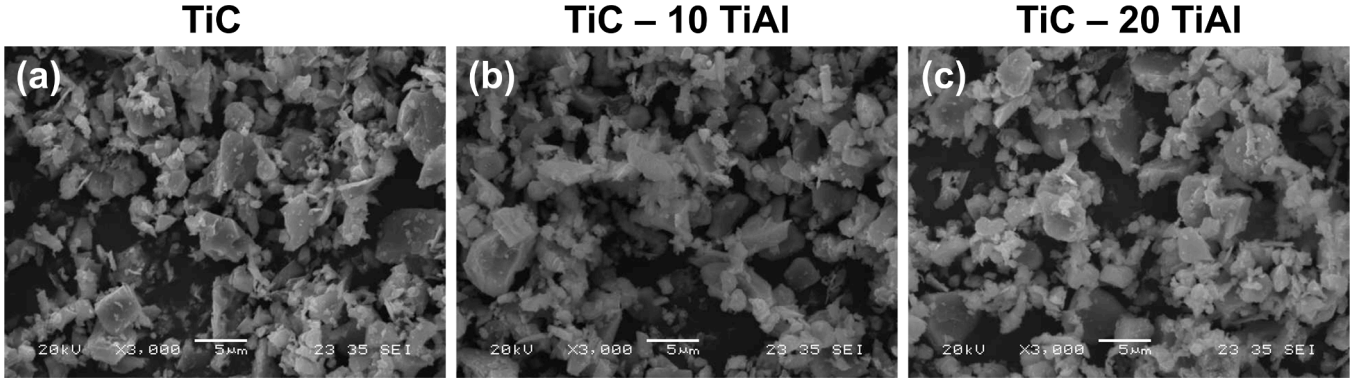

Fig. 1. Morphology of the starting powders used for the flash sintering experiments.

hole drilled in the mid-thickness of the hBN die. The pyrometer measured a temperature of ~ 2000 °C in 15 – 18 s for all experiments carried out under 5 V voltage.

2.3. Materials characterization

The density of the sintered samples was measured by the Archimedes' principle, with water as a buoyant medium. Measurements were carried out using an analytical balance with a sensitivity of 0.1 mg.

The sintered samples were sectioned into two halves along the longitudinal axis and used for Scanning Electron Microscopy (SEM), X-ray Diffraction (XRD) analysis, and Vickers hardness measurements.

One of the sections was embedded in epoxy resin and subsequently ground and polished using diamond paste down to a 1 μm grain size; microstructural analysis was carried out by SEM (JEOL JSM-IT300LV, Tokyo, Japan) equipped with an Energy-dispersive X-ray spectroscopy microprobe (Bruker XFlash 630 M detector, Germany) operating at 20 keV after sputter-coating the samples with a thin Pt–Pd layer.

XRD was carried out on the flat surface of the longitudinally sectioned samples using an Italstructures IPD3000 diffractometer with a copper anode source ($\lambda = 1.5406$ Å, 40 kV, 30 mA).

Vickers hardness was measured using a Tecmet Future-Tech FM-310 microhardness tester (Italy) with a load of 0.2 kgf, with an average of 5 measurements per sample.

3. Results

Fig. 3(a-b) shows the optical images and their corresponding flash sintering curves of TiC – 10TiAl and TiC – 20TiAl samples, processed at an applied voltage of 5 V, a dwell time of 30 s, and an applied pressure of 20 MPa. As with any flash event, our experiments are characterized by an incubation period with a sharp increase in power dissipation accompanied by a rapid shrinkage. Although both compositions exhibit similar average power dissipation during the flash event, a distinct difference in shrinkage behaviour is evident. The TiC – 20TiAl composition exhibits considerably greater shrinkage compared to the TiC – 10TiAl sample (Fig. 3(b)). For instance, TiC–20TiAl sample undergoes substantially greater shrinkage, achieving ~25%-dimensional reduction compared to ~17% for TiC – 10TiAl. This trend is also evident in the optical images (Fig. 3(a)), where the height decreases from 9.7 mm in the green state to ~7.86 mm and ~7.23 mm for TiC – 10TiAl and TiC – 20TiAl (flash sintered samples), respectively.

Fig. 4(a-b) depicts the power–time profiles of TiC – 10TiAl and TiC – 20TiAl samples subjected to flash sintering under different applied pressures, with a constant applied voltage of 5 V. For the TiC – 10TiAl composition (Fig. 4(a)), the incubation period preceding the flash event consistently decreases as the applied pressure increases. Following flash onset, all pressure conditions exhibit similar levels of power dissipation, with only slight variations observed during the holding phase. A similar pattern is also evident for the TiC – 20TiAl composition (Fig. 4(b)), where the incubation period similarly diminishes as the applied pressure increases.

As shown in Fig. 5, the incubation time is strongly influenced by both composition and applied pressure. For all investigated pressure levels, the TiC–20TiAl samples exhibit longer incubation times than the corresponding TiC–10TiAl samples. In the context of flash sintering, the incubation period is defined as the waiting time just before the occurrence of the flash event [33]. For instance, for TiC – 10TiAl, the incubation time decreases from approximately 10 s at 20 MPa to less than 3 s at 60 MPa, while TiC – 20TiAl shows a reduction from approximately 15 s to about 3 s over the same pressure range. These observations indicate that pressure primarily influences flash initiation by improving electrical contact between particles, whereas the subsequent thermal regime is governed mainly by Joule heating.

The relative density and open porosity of pure TiC, TiC – 10TiAl, and TiC – 20TiAl samples flash sintered under various voltage, pressure, and holding time conditions are summarized in Fig. 6 and Table 3. The relative density increases with holding time for both the TiC – 10TiAl and TiC – 20TiAl compositions. TiC – 20TiAl samples achieve greater relative densities than TiC – 10TiAl samples under similar processing conditions. The highest relative density obtained in this study is 91.2 ± 1.5% for TiC – 20TiAl processed for 60 s at 5 V and 40 MPa. Under similar conditions, TiC – 10TiAl reaches only 77.3 ± 2.6%, indicating that increasing the TiAl content results in a relative density increase of ~15%. As the relative density increases, the corresponding open porosity values decrease. In comparison to the TiC – TiAl composites, pure TiC samples treated under the same conditions exhibit larger open porosity and lower relative density (78.5 ± 3.1%), thereby demonstrating the effectiveness of the sintering aid. In addition, the applied pressure does not appear to significantly affect the final densification process, suggesting that densification is governed predominantly by the thermal conditions generated during flash sintering rather than by the externally applied pressure.

Fig. 7(a-c) reports the X-ray diffraction patterns of pure TiC, TiC – 10TiAl, and TiC – 20TiAl powders, together with the flash-sintered samples. The diffraction patterns of the as-received powders indicate that TiC is the predominant phase, accompanied by additional low-intensity peaks corresponding to TiAl, as marked with blue circles in

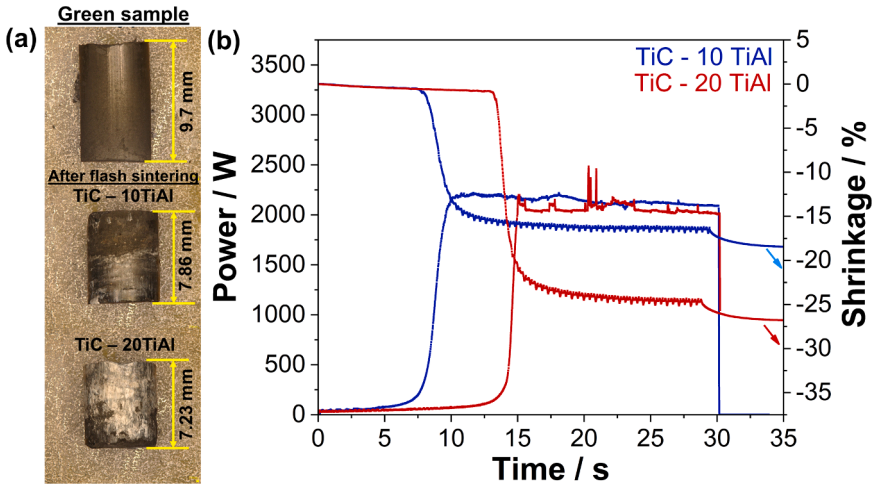

Fig. 3. (a) Optical images of the uniaxially pressed and flash sintered samples. (b) Evolution of power and shrinkage during the flash sintering experiment, highlighting the effect of the secondary TiAl amount. The voltage was set to 5 V and the pressure to 20 MPa.

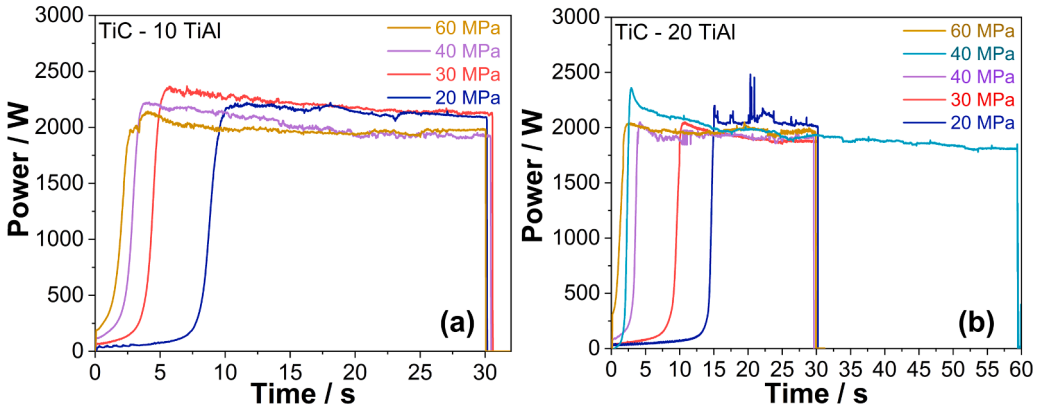

Fig. 4. Power-time curves for TiC with (a) 10 vol% TiAl, and (b) 20 vol% TiAl as a function of the applied pressure during the flash sintering experiments. The voltage was set to 5 V.

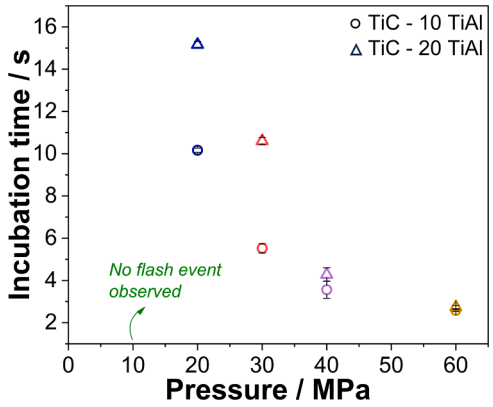

Fig. 5. Incubation time as a function of the applied pressure during the flash sintering experiments.

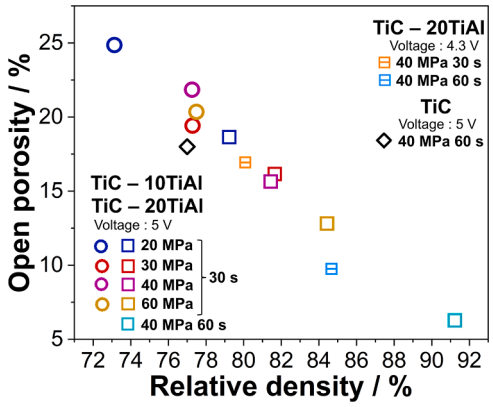

Fig. 6. Variation of density and open porosity of the flash-sintered samples as a function of voltage, pressure, and holding time.

Fig. 7(b-c). Since TiAl, $TiAl_2$, and $TiAl_3$ have comparable diffraction patterns, it is impossible to pinpoint the precise stoichiometry of the aluminide; therefore, we will refer to it as $TiAl_y$ [22]. Post-flash sintering, the diffraction patterns of both TiC – 10TiAl and TiC – 20TiAl samples are characterised by TiC reflections (JCPDS: 00–031–1400). No additional peaks are observed in the sintered samples compared to the initial powders. The absence of distinct TiAl reflections in the sintered samples suggests either oxidation into phases below the XRD detection limit, or partial loss of aluminium during processing. These observations are supported by the EDS results discussed later (Fig. 9).

Fig. 8 shows SEM micrographs (in back-scattered mode) of pure TiC and TiC – TiAl composites sintered at 40 MPa with different durations. The pure TiC sample sintered for 60 s demonstrates a microstructure characterized by irregularly shaped grains and a significant proportion of interconnected porosity, a characteristics feature of incomplete sintering (Fig. 8(a)). The incorporation of TiAl results in a significant enhancement in microstructural development. The TiC – 10TiAl sample sintered for 30 s exhibits enhanced interparticle bonding and coarsening relative to pure TiC; yet, with the presence of interconnected porosity (Fig. 8(b)). No substantial amount of secondary phase could be observed. An additional increase in TiAl concentration to 20 vol% leads to a more consolidated microstructure after 30 s, characterised by a significant decrease in the interconnected porosity with a visible secondary phase (Fig. 8(c)). Prolonging the dwell period to 60 s for the TiC – 20TiAl composition yields the densest microstructure, distinguished by isolated residual porosity and the presence of the secondary phase (Fig. 8(d)). Additionally, the existence of the secondary TiAl phase is shown to drastically change the grain shape during sintering. The TiC – 20TiAl sample that was sintered for 60 s at 40 MPa exhibits more equiaxed and rounded grain morphologies (Fig. 8(d)) than pure TiC, which mostly displays irregular and angular grains (Fig. 8(a)).

Fig. 9 shows the EDXS elemental maps of Ti, Al, and O for pure TiC and TiC – TiAl composites sintered under 40 MPa and variable times. The pure TiC sample (60 s) exhibits a uniform distribution of Ti (Fig. 9(a)). For the TiC – 10TiAl sample sintered for 30 s, Al-rich regions appear to be present in the Ti matrix as clusters (Fig. 9(b)). For compositions with 20 vol% TiAl, the Al signal becomes more intense and shows localized enrichment at specific regions, while Ti maintains a relatively uniform distribution (Fig. 9(c-d)). The oxygen signal partially overlaps with Al-enriched areas, suggesting the presence of oxides. However, prolonged treatment results in a reduction in the amount of Al-containing regions (Fig. 9(d)).

The EDXS line-scan shown in Fig. 9(e) for the TiC – 20TiAl sample indicates that the dark regions are characterized by a decrease in Ti intensity and a corresponding increase in Al intensity. However, Al enrichment is not always uniformly associated with the presence of oxygen. Table 2 summarizes the Al content obtained from EDXS analysis. Although EDXS provides only semi-quantitative compositional information, a clear reduction in Al signal is observed after sintering, indicating that approximately 70% of the Al is lost during sintering. Interestingly, the measured aluminium loss remains relatively constant despite increasing the holding time from 30 to 60 s. This observation suggests that most aluminium evaporation and oxidation occur during the initial flash event, when the temperature and heating rate are highest, rather than during the subsequent holding period.

The Vickers hardness of the sintered samples reported in Table 3 and Fig. 10 suggests that, although the densification of TiC was limited to

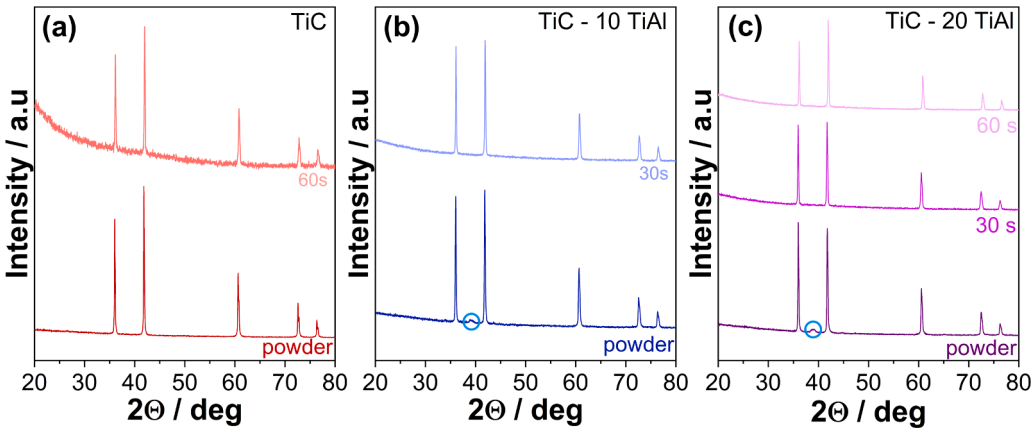

Fig. 7. X-ray diffraction (XRD) patterns of the synthesized powder and the flash sintered samples processed at a voltage of 5 V and a pressure of 40 MPa.

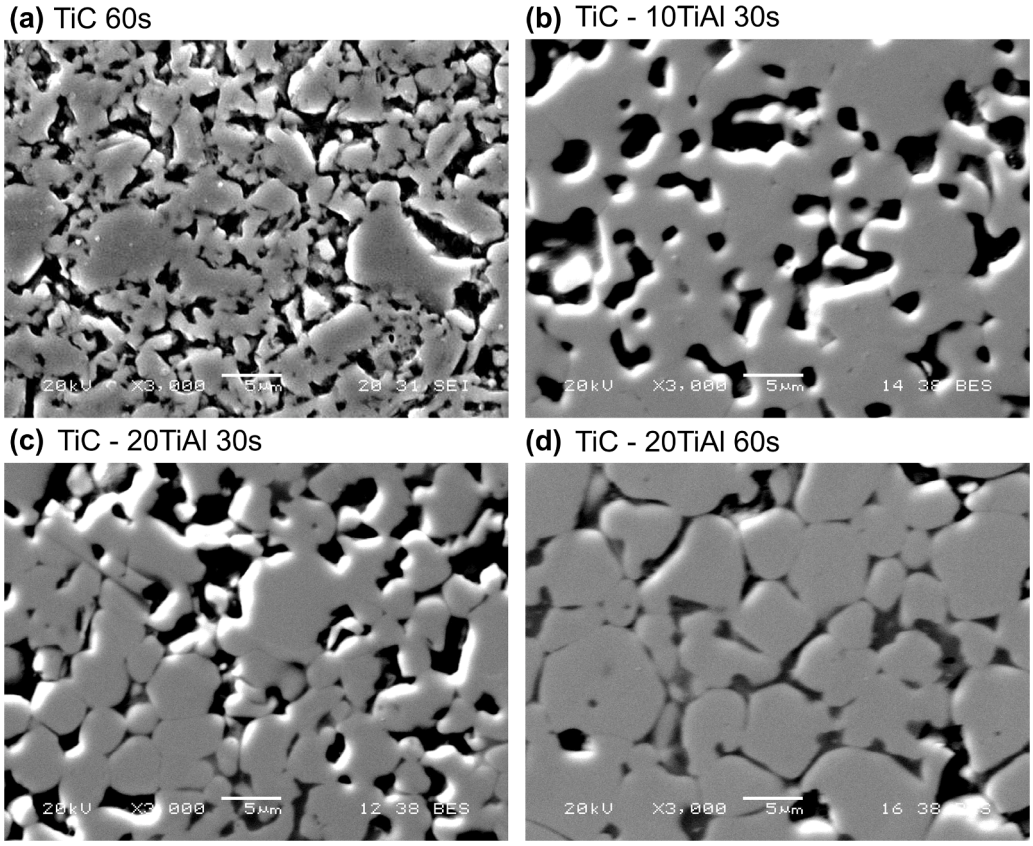

Fig. 8. Microstructural analysis of the flash sintered samples: (a) Pure TiC for 60 s, (b) TiC with 10 vol% TiAl for 30 s, and TiC with 20 vol% TiAl for (c) 30 s, and (d) 60 s. All samples are sintered at 5 V with a pressure of 40 MPa.

78%, its hardness remains high due to the intrinsically high hardness of the TiC powder. With increasing TiAl content and holding time, the hardness increases and reaches a maximum of ~13 GPa for TiC –20TiAl sintered for 60 s. Owing to the significant porosity of the samples, the measured Vickers hardness values may lack absolute accuracy but still provide useful comparative trends.

4. Discussion

In a typical flash sintering experiment on NTC ceramics, the application of an electric field at a sufficiently high furnace temperature allows electrical current to pass through the sample. This leads to a rapid increase in power dissipation due to Joule heating, resulting in almost instantaneous shrinkage and near-full densification within a few seconds, accompanied by extremely high heating rates. A similar behaviour is also observed in the present work for TiC at room temperature, which is a PTC ceramic (Fig. 3,4).

The electrical parameters play a crucial role in determining both the peak power and the steady-state power dissipation during flash sintering. In the present study, the applied voltage was used as the primary control parameter. A voltage of 5 V was selected to allow a higher current to pass through the green compact, resulting in a higher steady-state power dissipation. It is important to note that increasing the voltage to 6 V leads to the melting of the molybdenum electrodes. Although the pyrometer indicated a temperature of ~2000 °C, the actual sample temperature is expected to be higher, since the pyrometer was

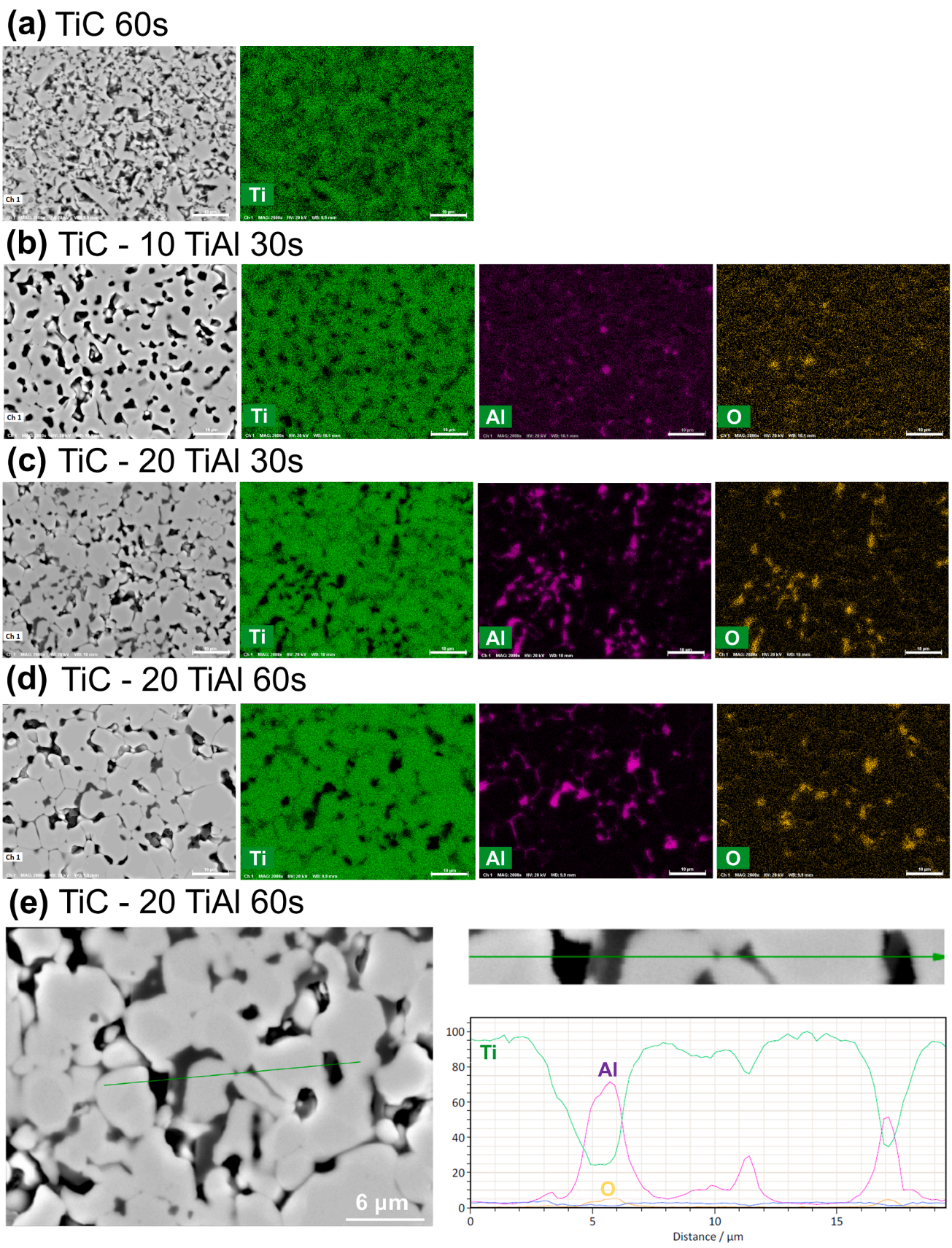

Fig. 9. EDXS maps showing the elemental distribution in the flash sintered samples: (a) Pure TiC for 60 s, (b) TiC with 10 vol% TiAl for 30 s, and TiC with 20 vol% TiAl for (c) 30 s, and (d) 60 s. The scale bar in all images (a–d) corresponds to 10 µm. (e) EDXS line-scan in TiC with 20 vol% TiAl for 60 s. All samples are sintered at 5 V and a pressure of 40 MPa.

Table 2
Comparing the semi-quantitative compositional information of the Al lost during the flash sintering process. The samples were processed at 5 V and a pressure of 40 MPa.

Sample	Aluminium [Al] in wt% from EDS	Theoretical amount of [Al] in wt%	Weight fraction of Al lost during sintering in %
TiC 60s	0	0	
TiC 10 TiAl 30 s	0.7 ± 0.1	2.9	~ 75
TiC 20 TiAl 30 s	1.8 ± 0.1	6.0	~ 71
TiC 20 TiAl 60 s	1.4 ± 0.1	6.0	~ 77

Table 3
The relative density and Vickers hardness of the flash sintered samples processed at 5 V and pressure 40 MPa.

Sample	Relative density (%)	Vickers Hardness (GPa)
TiC 60s	78.5 ± 3.1	16.2 ± 1.9
TiC 10 TiAl 30s	77.3 ± 2.6	8.2 ± 1.4
TiC 20 TiAl 30s	81.4 ± 2.9	10.1 ± 1.2
TiC 20 TiAl 60s	91.2 ± 1.5	13.2 ± 1.0

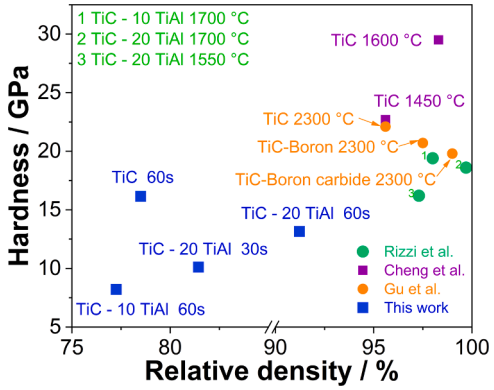

Fig. 10. Hardness as a function of relative density for the flash-sintered samples processed in this work at 5 V and an applied pressure of 40 MPa. The results obtained in this study are compared with selected literature data for samples processed using SPS (Ref no [18,22,23]).

focused on the die rather than directly on the sample, and heat losses to the surroundings should also be considered. Nevertheless, the heating rate can be approximated in the order of 10^3 °C/min, which is in good agreement with the literature.

It is interesting to note that our experiments revealed two distinct characteristics. First, the applied pressure has a significant influence on the incubation time: with an increase in the applied pressure, the time required to reach the power peak decreases (Figs. 4,5). This behaviour can be attributed to the effect of pressure on the initial electrical resistivity of the green compact, which is determined by the contact area between adjacent particles. Higher applied pressure increases the actual interparticle contact area, lowering the contact resistance and facilitating current flow through the compact [34,35]. One could argue that applying pressure to the electrodes increases green density, and thus improves current flow. However, a relatively high pressure was already applied during compaction, while the pressure used during flash sintering was limited to 20 – 60 MPa.

Considering that the flash event leads to estimated temperatures approaching 2000 °C within a few seconds, densification is likely governed primarily by rapid Joule heating and liquid-phase formation rather than by externally applied pressure. Although pressure influences the incubation time by modifying interparticle contact resistance, its effect on final densification appears limited once thermal runaway is established.

The second notable feature was the increase in the incubation time with an increase in the TiAl content (Fig. 5). Compared to TiC, TiAl exhibits lower electrical conductivity at room temperature and elevated temperatures [36,37]. This implies that the connectivity of the conductive TiC network is disrupted by an increase in the TiAl content, which can result in a delay in the establishment of a continuous current percolation path. Moreover, TiAl has been reported to undergo plastic deformation under applied pressure and elevated temperature [38], allowing it to accommodate strain during initial heating and potentially delaying the onset of localised thermal instabilities.

The densification of the sintered samples is primarily governed by the amount of sintering aid and the holding time (Fig. 6). While the applied pressure does not show a significant influence on the densification behaviour, a pressure of 10 MPa was insufficient to initiate the flash process, as the low pressure did not ensure adequate contact between the electrodes and the sample. A pressure of 20 MPa appeared to be sufficient; however, large noise was observed (Fig. 3(b), Fig. 4(b)), likely due to poor contact. Therefore, a higher pressure of 40 MPa was selected to ensure better electrical contact and produce the final set of samples for analysis. The density of the sintered samples increased with increasing TiAl content, as clearly shown in Fig. 6. This observation suggests that TiAl acts as an effective sintering aid, facilitating densification through the formation of a transient liquid-phase leading to more rounded grains compared to the irregularly shaped grains observed in pure TiC (Fig. 8,9).

Pure TiC exhibits inherently limited sinterability as a result of its strong covalent bonding and low self-diffusion rates, which restrict mass transport during short dwell times and lead to insufficient neck development and a high level of residual porosity. The incorporation of TiAl alters the densification behaviour by introducing a phase with significantly higher diffusion capability, thereby facilitating the particle rearrangement under the applied pressure. During sintering, the TiAl phase may undergo localized melting, which improves its ability to wet TiC particles, enhances interparticle contact, and accelerates neck growth between adjacent grains. An increase in TiAl content further amplifies these effects by increasing the fraction of the diffusion-active phase, promoting more effective pore closure and grain consolidation. Extending the holding time allows these mechanisms to progress more fully, enabling continued mass transport and pore shrinkage, and ultimately resulting in a more densified microstructure.

As shown in Fig. 6, the maximum relative density was approximately 91% for the composites with 20 vol% TiAl. When compared to other reports on the sintering of TiC, this value might seem low. However, it is crucial to keep in mind that the initial powder properties, specifically the particle size, have a significant impact on the densification kinetics [39]. In the present work, TiC particles were relatively coarse (micrometric range < 5 μm). Since the driving force for sintering is directly related to the curvature of the particle surface, coarser particles exhibit a lower surface curvature, leading to a reduced sintering driving pressure and therefore slower densification [40]. Moreover, it should be emphasized that the present densification was achieved under an extremely rapid thermal cycle and, importantly, in air. This processing route is significantly faster than conventional pressure-assisted techniques such as Spark Plasma Sintering and Hot Pressing, which are typically conducted under inert or vacuum conditions.

EDXS analysis reveals that, after sintering, TiAl (T_m= 1460 °C) does not remain fully in its original form as depicted in Fig. 9. Given its relatively low melting temperature compared to the sintering temperature, TiAl is expected to melt at an early stage, thereby promoting liquid phase sintering and contributing to the initial densification of the

composite. At elevated temperatures, aluminium exhibits high vapor pressure and strong oxygen affinity; consequently, partial evaporation and oxidation occur, leading to the formation of Al_2O_3. This interpretation is consistent with the data presented in Tables 2 and 3. For the composite containing 20 vol% TiAl, the relative density increases from 81.4% to 91.2% as the holding time is extended from 30 to 60 s, whereas the Al loss remains nearly unchanged. This suggests that most TiAl decomposition and oxidation occur during the initial stage of flash sintering. The resulting alumina, having a much higher melting temperature (T_m= 2050 °C), remains stable at higher temperatures and function as a refractory phase after the transient liquid phase, thereby contributing to high-temperature stability of the composite.

Nevertheless, alumina was not observed in the XRD patterns (Fig. 7), most likely due to its content being below the detection limit of the instrument. The Al content in the sintered samples, as reported in Table 2, was significantly lower than the corresponding theoretical value, indicating that TiAl is partially lost during sintering or transformed into alumina. The latter is supported by the EDS elemental maps shown in Fig. 9(e), which reveal Al–O–rich regions consistent with the formation of Al_2O_3. At the same time, Al enrichment is observed within and around the residual pores, suggesting that Al-containing phases are expelled from the bulk due to the application of pressure and redistributed during sintering. This behaviour is likely promoted by the combined effects of rapid heating and applied pressure, leading to extrusion or migration of the Al-rich phase toward the pore channels. Such redistribution also provides a plausible explanation for the increased shrinkage observed in the TiC – 20 vol% TiAl composite, where the larger fraction of a deformable Al-containing phase enhances particle rearrangement and pore collapse during densification.

The reported hardness values for the sintered composites are still low compared to those of pure TiC, even though the latter has a lower density. This can be attributed to the lower hardness values of TiAl or Al_2O_3 when compared to TiC. The measured hardness values are also lower than those reported in the literature (Fig. 10; Table 3) for both TiC and TiC-based composites, suggesting that the comparatively lower densification achieved in this study is the primary factor governing the reduced hardness.

5. Conclusion

The present work demonstrates that TiC can be flash sintered in air in a very short time, especially when TiAl is added. The composite containing 20 vol.% TiAl achieved a relative density of approximately 90% in 60 s. Such an achievement is particularly remarkable considering the long processing times typically required to process such materials using conventional techniques. No other phases apart from TiC are observed although EDXS analysis reveals the presence of aluminium oxide. Future studies should focus on enhancing the density of the sintered composites but the results of the present work point out the possibility of producing ultra-high temperature ceramics using very simple equipment and by using limited amount of energy.

CRediT authorship contribution statement

Subhadip Bhandari: Writing – review & editing, Writing – original draft, Visualization, Validation, Methodology, Investigation, Funding acquisition, Formal analysis, Data curation, Conceptualization. **Milad Kermani:** Writing – review & editing, Methodology, Investigation, Conceptualization. **Mattia Biesuz:** Writing – review & editing, Validation, Supervision. **Vincenzo M. Sglavo:** Writing – review & editing, Validation, Supervision, Resources, Project administration, Conceptualization.

Declaration of competing interest

The authors declare the following financial interests/personal relationships which may be considered as potential competing interests: Subhadip Bhandari reports financial support was provided by Journal of European Ceramic Society Trust. If there are other authors, they declare that they have no known competing financial interests or personal relationships that could have appeared to influence the work reported in this paper.

Acknowledgement

Subhadip Bhandari gratefully acknowledges the JECS trust (Contract **2023 369 – 03** and Contract **2023 369 22**) for the financial support to attend the ICACC conference at Daytona Beach, Florida, USA. The authors would like to thank Prof. Rodrigo Moreno (Institute of Ceramics and Glass, Spanish National Research Council – CSIC) for providing the powders and for his constructive feedback on the manuscript.

References

[1] M. Biesuz, S. Grasso, V.M. Sglavo, What's new in ceramics sintering? A short report on the latest trends and future prospects, Curr. Opin. Solid. State Mater. Sci. 24 (2020) 100868, https://doi.org/10.1016/J.COSSMS.2020.100868.
[2] D. Liu, G. Shao, X. Tai, X. Li, S.C. Jeon, J. Guo, M. Lin, W. Ji, Y. Xiong, S. Chen, F. Zuo, S. Grasso, H.T. Lin, X. Wang, X. Su, K. Ren, Y. Liu, J. Liu, Field-assisted sintering: overview of thermo-electro-mechanical coupling effects, J. Adv. Ceram. 15 (2026) 9221276, https://doi.org/10.26599/JAC.2026.9221276.
[3] M. Cologna, B. Rashkova, R. Raj, Flash sintering of Nanograin Zirconia in <5 s at 850°C, J. Am. Ceram. Soc. 93 (2010) 3556–3559, https://doi.org/10.1111/J.1551-2916.2010.04089.X.
[4] M. Biesuz, V.M. Sglavo, Flash sintering of alumina: effect of different operating conditions on densification, J. Eur. Ceram. Soc. 36 (2016) 2535–2542, https://doi.org/10.1016/J.JEURCERAMSOC.2016.03.021.
[5] S. Bhandari, T.P. Mishra, M. Bram, O. Guillon, D. Yadav, Flash sintering behaviour of 8YSZ-NiO composites, Ceram. Int. 48 (2022) 33236–33244, https://doi.org/10.1016/J.CERAMINT.2022.07.266.
[6] S. Bhandari, T.P. Mishra, O. Guillon, D. Yadav, M. Bram, Accessing the role of Joule heating on densification during flash sintering of YSZ, Scr. Mater. 211 (2022) 114508, https://doi.org/10.1016/J.SCRIPTAMAT.2022.114508.
[7] R.I. Todd, E. Zapata-Solvas, R.S. Bonilla, T. Sneddon, P.R. Wilshaw, Electrical characteristics of flash sintering: thermal runaway of joule heating, J. Eur. Ceram. Soc. 35 (2015) 1865–1877, https://doi.org/10.1016/J.JEURCERAMSOC.2014.12.022.
[8] A. Eqbal, K.S. Arya, T. Chakrabarti, In-depth study of the evolving thermal runaway and thermal gradient in the dog bone sample during flash sintering using finite element analysis, Ceram. Int. 46 (2020) 10370–10378, https://doi.org/10.1016/J.CERAMINT.2020.01.034.
[9] M. Biesuz, V.M. Sglavo, Flash sintering of ceramics, J. Eur. Ceram. Soc. 39 (2019) 115–143, https://doi.org/10.1016/J.JEURCERAMSOC.2018.08.048.
[10] M. Yu, S. Grasso, R. Mckinnon, T. Saunders, M.J. Reece, Review of flash sintering: materials, mechanisms and modelling, Adv. Appl. Ceram. 116 (2017) 24–60, https://doi.org/10.1080/17436753.2016.1251051.
[11] C.E.J. Dancer, Flash sintering of ceramic materials, Mater. Res. Express. 3 (2016) 102001, https://doi.org/10.1088/2053-1591/3/10/102001.
[12] I.R. Lavagnini, J.V. Campos, E.M.J.A. Pallone, Microstructure evaluation of 3YSZ sintered by two-step flash sintering, Ceram. Int. 47 (2021) 21618–21624, https://doi.org/10.1016/j.ceramint.2021.04.174.
[13] A. Eqbal, R. Raj, S.K. Singh, A. Gupta, S.K. Jha, T. Chakrabarti, Study on structural and microstructural evolution during liquid phase flash sintering of 3mol% yttria stabilized zirconia, J. Eur. Ceram. Soc. 45 (2025) 117408, https://doi.org/10.1016/J.JEURCERAMSOC.2025.117408.
[14] I. Mazo, B. Palmieri, A. Martone, M. Giordano, V.M. Sglavo, Flash sintering in metallic ceramics: finite element analysis of thermal runaway in tungsten carbide green bodies, J. Mater. Res. Technol. 23 (2023) 5993–6004, https://doi.org/10.1016/j.jmrt.2023.02.213.
[15] H.O. Pierson, Handbook of refractory carbides and nitrides : properties, characteristics, Process. Appl. (1996) 340.
[16] M. Mhadhbi, Titanium carbide: synthesis, properties and applications, Brill. Eng. 2 (2020) 1–11, https://doi.org/10.36937/ben.2021.002.001.
[17] M. Shahedi Asl, Z. Ahmadi, A. Sabahi Namini, A. Babapoor, A. Motallebzadeh, Spark plasma sintering of TiC–SiCw ceramics, Ceram. Int. 45 (2019) 19808–19821, https://doi.org/10.1016/J.CERAMINT.2019.06.236.
[18] Y. Gu, J.X. Liu, F. Xu, G.J. Zhang, Pressureless sintering of titanium carbide doped with boron or boron carbide, J. Eur. Ceram. Soc. 37 (2017) 539–547, https://doi.org/10.1016/J.JEURCERAMSOC.2016.08.035.
[19] L. Liang, B. Wei, M. Zhang, W. Fang, L. Chen, Y. Wang, Novel TiC-based ceramic with enhanced mechanical properties by reaction hot-pressing at low temperature, J. Mater. Res. Technol. 24 (2023) 2129–2143, https://doi.org/10.1016/J.JMRT.2023.03.111.
[20] A. Sabahi Namini, Z. Ahmadi, A. Babapoor, M. Shokouhimehr, M. Shahedi Asl, Microstructure and thermomechanical characteristics of spark plasma sintered TiC ceramics doped with nano-sized WC, Ceram. Int. 45 (2019) 2153–2160, https://doi.org/10.1016/J.CERAMINT.2018.10.125.

[21] A. Babapoor, M.S. Asl, Z. Ahmadi, A.S. Namini, Effects of spark plasma sintering temperature on densification, hardness and thermal conductivity of titanium carbide, Ceram. Int. 44 (2018) 14541–14546, https://doi.org/10.1016/J.CERAMINT.2018.05.071.
[22] A. Rizzi, M. García-Fernández, M. Rodríguez, E. De Bona, R. Moreno, M. Biesuz, Spark plasma sintering of TiC with TiAly as sintering aid: mechanisms and microstructures, Open Ceram. 19 (2024) 100661, https://doi.org/10.1016/J.OCERAM.2024.100661.
[23] L. Cheng, Z. Xie, G. Liu, W. Liu, W. Xue, Densification and mechanical properties of TiC by SPS-effects of holding time, sintering temperature and pressure condition, J. Eur. Ceram. Soc. 32 (2012) 3399–3406, https://doi.org/10.1016/J.JEURCERAMSOC.2012.04.017.
[24] B.M. Moshtaghioun, R.C. Crespo, F.L. Cumbrera, D. Gómez-García, M. G. Fernández, M.A. Rodríguez, R. Moreno, Mechanical performance of sub-stoichiometric titanium carbide ceramics synthesized by a hybrid SHS and SPS methodology, J. Eur. Ceram. Soc. 46 (2026) 117748, https://doi.org/10.1016/J.JEURCERAMSOC.2025.117748.
[25] M. Maurya, S. Kumar, A. Maurya -, Y. Wenle, F. Ruicheng, Z. Baocheng, X. Zhu, M. Yang, M. Luo, Z. Sun, L. Yang, S. Wang, Q. Wang, Effect of TiC and TiB2 content on properties of TiAl based alloys, IOP Conf. Ser. Earth Env. Sci. 714 (2021) 032005, https://doi.org/10.1088/1755-1315/714/3/032005.
[26] X. Chen, C. Li, X. Bai, H. Liu, S. Xu, Y. Hu, Microstructure, Microhardness, Fracture toughness, and abrasive wear of In-situ synthesized TiC/Ti-Al composite coatings by cold spraying combined with heat treatment, Coatings 11 (2021) 1034, https://doi.org/10.3390/COATINGS11091034.
[27] H.C. Yi, J.J. Moore, Self-propagating high-temperature (combustion) synthesis (SHS) of powder-compacted materials, J. Mater. Sci. 25 (1990) 1159–1168, https://doi.org/10.1007/BF00585421/METRICS.
[28] Z.A. Munir, U. Anselmi-Tamburini, Self-propagating exothermic reactions: the synthesis of high-temperature materials by combustion, Mater. Sci. Rep. 3 (1989) 277–365, https://doi.org/10.1016/0920-2307(89)90001-7.
[29] S.K. Mishra, L.C. Pathak, Self-propagating high-temperature synthesis (SHS) of advanced high-temperature ceramics, Key. Eng. Mater. 395 (2009) 15–38, https://doi.org/10.4028/WWW.SCIENTIFIC.NET/KEM.395.15.
[30] I. Mazo, A. Molinari, V.M. Sglavo, Electrical resistance flash sintering of tungsten carbide, Mater. Des. 213 (2022) 110330, https://doi.org/10.1016/j.matdes.2021.110330.
[31] I. Mazo, A. Molinari, V.M. Sglavo, Effect of pressure on the electrical resistance flash sintering of tungsten carbide, J. Eur. Ceram. Soc. 42 (2022) 2028–2038, https://doi.org/10.1016/j.jeurceramsoc.2022.01.017.
[32] V.M. Sglavo, E. De Bona, I. Mazo, Flash sintering of metal-like ceramics: a short overview, Ceram. Int. 50 (2024) 37356–37365, https://doi.org/10.1016/j.ceramint.2024.05.018.
[33] C. Singh, D. Yadav, Densification during Stage I: the incubation period in flash sintering, J. Am. Ceram. Soc. 109 (2026) e70566, https://doi.org/10.1111/JACE.70566.
[34] R. Chaim, Numerical model for particle size effects on flash sintering temperature of ionic nanoparticles, J. Mater. Sci. 53 (2018) 13853–13864, https://doi.org/10.1007/S10853-018-2604-X/FIGURES/6.
[35] J.S.C. Francis, R. Raj, Flash-sinterforging of Nanograin Zirconia: field assisted sintering and superplasticity, J. Am. Ceram. Soc. 95 (2012) 138–146, https://doi.org/10.1111/J.1551-2916.2011.04855.X.
[36] J.G. Li, B.C. Wei, M.X. Pan, D.Q. Zhao, Y.G. Zhang, C.Q. Chen, The relationship between resistivity and temperature in ordered α2-Ti3Al and γ-TiAl intermetallic compounds single crystals, Mater. Sci. Eng. 268 (1999) 193–196, https://doi.org/10.1016/S0921-5093(99)00070-2.
[37] G. Drendel, E.R. Mathews, L. Semenec, A.E. Franks, The effect of TiC additive on mechanical and electrical properties of Al2O3 ceramic, Appl. Sci. 8 (2018) 2385, https://doi.org/10.3390/APP8122385.
[38] H.A. Soliman, J. Pineault, M. Elbestawi, Influence of combined heat treatment and hot isostatic pressure (HT-HIP) on titanium aluminide processed by L-PBF, Materials 16 (2023) 5071, https://doi.org/10.3390/MA16145071.
[39] J.S.C. Francis, M. Cologna, R. Raj, Particle size effects in flash sintering, J. Eur. Ceram. Soc. 32 (2012) 3129–3136, https://doi.org/10.1016/J.JEURCERAMSOC.2012.04.028.
[40] M. Barsoum, M.W. Barsoum, Fundamentals of ceramics, (2002). https://doi.org/10.1201/B21299.